J Mater Sci (2009) 44:2109–2118
DOI 10.1007/s10853-009-3299-9

Numerical analysis for migration of austenite/ferrite interface during carburization of Fe

M. Kajihara

Received: 31 May 2008 / Accepted: 26 January 2009 / Published online: 26 February 2009

Abstract During isothermal annealing of the ferrite of a binary Fe–C alloy in an appropriate carburization atmosphere at temperatures of 1020–1180 K, the austenite will be formed as a layer on the surface of the ferrite. The migration behavior of the austenite/ferrite interface during the isothermal carburization was numerically analyzed using the diffusion equation describing the flux balance at the interface. However, the diffusion coefficient of C in the austenite monotonically increases with increasing concentration of C. Thus, the composition dependence of the diffusion coefficient was taken into consideration. For the numerical analysis, Crank–Nicolson implicit method was combined with a finite-difference technique. According to the numerical calculation, the parabolic relationship holds between the migration distance of the austenite/ferrite interface and the annealing time. The composition dependence of the diffusion coefficient yields acceleration of the migration. The numerical calculation satisfactorily reproduces the experimental result of the diffusion controlling migration.

Introduction

The reactive diffusion between different pure metals or alloys has been experimentally observed by many investigators [1–51]. In such an experiment, a semi-infinite diffusion couple may be isothermally annealed at an appropriate temperature where diffusion occurs considerably. Here, the semi-infinite diffusion couple means that the thickness is semi-infinite for the constituent specimens and the interface is flat. Due to annealing, some of the stable intermediate phases will be produced as layers along the interface. If the growth of the intermediate layers is controlled by volume diffusion, the square of the total thickness of the intermediate layers is proportional to the annealing time as long as the diffusion couple is semi-infinite [52]. Such a relationship is called the parabolic relationship. In order to examine the characteristic features of the parabolic relationship, the kinetics of the reactive diffusion controlled by volume diffusion was quantitatively analyzed in previous studies [53–60]. In these analyses, different binary alloy systems consisting of one intermediate phase and two primary solid-solution phases were treated, and the diffusion coefficient of each phase was assumed to be independent of the composition. Under such conditions, the growth rate of the intermediate layer was evaluated for various semi-infinite diffusion couples initially composed of the two primary solid-solution phases. Since the diffusion coefficient is only a function of the temperature, the evaluation can be carried out analytically.

On the other hand, the carburization of Fe was experimentally studied by Togashi and Nishizawa [61]. In their experiment, a pure Fe specimen of the ferrite (α) phase with the body-centered-cubic (bcc) structure was isothermally annealed at 1073 K for various periods up to 9 h in a carburization atmosphere with the same activity of C as graphite. During annealing, the austenite (γ) phase with the face-centered-cubic (fcc) structure is formed on the α phase, and gradually grows into the α phase. Since the γ/α interface migrates according to the parabolic relationship at annealing times longer than 2 h, the migration is controlled by the volume diffusion of C in the α and γ phases. However, the diffusion coefficient of C in the γ phase of the

M. Kajihara (✉)
Department of Materials Science and Engineering, Tokyo Institute of Technology, Nagatsuta 4259-J2-59, Midori-ku, Yokohama 226-8502, Japan
e-mail: kajihara@materia.titech.ac.jp

binary Fe–C system varies depending on the chemical composition [62, 63]. The composition dependence of the diffusion coefficient influences the flux balance between the γ and α phases and thus the migration rate of the γ/α interface. However, no reliable information is available for such influence. In this study, the migration behavior of the γ/α interface during carburization of the α phase in the binary Fe–C system was quantitatively analyzed using the diffusion equation describing the flux balance at the migrating interface. For the analysis, the composition dependence of the diffusion coefficient of C in the γ phase was taken into consideration. If the diffusion coefficient varies depending on the composition, however, the diffusion equation cannot be solved analytically. Thus, like previous studies [64, 65], a numerical technique was used for the quantitative analysis. The analysis satisfactorily explains the experimental result for the diffusion controlling migration of the γ/α interface reported by Togashi and Nishizawa [61].

Analysis

The equilibrium phase diagram in the binary Fe–C system was thermodynamically analyzed by Ågren [66], and then re-evaluated by Gustafson [67]. The re-evaluated phase diagram [67] is shown in Fig. 1. In this figure, the ordinate indicates the absolute temperature T, and the abscissa shows the mol fraction x of C. As can be seen, the temperatures T_3 and T_e of the A_3 $(\gamma \leftrightarrow \alpha)$ and eutectoid $(\gamma \leftrightarrow \alpha + \mathrm{gr})$ transformations are 1184.8 and 1011.2 K, respectively. In this figure, α, γ, and gr stand for the bcc-ferrite, fcc-austenite, and graphite phases, respectively, and $x^{\alpha\gamma}$, $x^{\gamma\alpha}$, and $x^{\gamma\mathrm{gr}}$ indicate the compositions of the $\alpha/(\alpha + \gamma)$, $\gamma/(\alpha + \gamma)$, and $\gamma/(\gamma + \mathrm{gr})$ phase boundaries, respectively.

Let us consider a semi-infinite diffusion couple initially consisting of a binary Fe–C alloy with the concentration $x^{\alpha 0}$ of C and a carburization atmosphere with the activity a_C of C. Thus, the diffusion couple is composed of the solid and gas phases. In the semi-infinite diffusion couple, the lengths of the alloy and the atmosphere are semi-infinite and the interface between them is flat. If the Fe–C alloy initially consists of the α phase, $x^{\alpha 0}$ is located in the α single-phase field of the phase diagram shown in Fig. 1. On the other hand, a_C is usually measured with a reference state of graphite. In such a case, a_C is equal to unity at $x = x^{\gamma\mathrm{gr}}$, but smaller than unity at $x < x^{\gamma\mathrm{gr}}$. When the diffusion couple is isothermally annealed in the temperature range of $T_e < T < T_3$ and a_C is greater than the value corresponding to $x = x^{\gamma\alpha}$, the γ phase will be formed as an intermediate layer with a uniform thickness of l at the interface between the α phase and the atmosphere. Here, the interface between a solid phase and an atmosphere is the surface of the solid phase. The concentration profile of C across the γ phase along the direction perpendicular to the surface of the γ phase is schematically shown in Fig. 2. Hereafter, this direction is denominated the diffusional direction. In Fig. 2, the ordinate shows the concentration c of C measured in mol per unit volume, and the abscissa indicates the distance z measured from the surface. The phase diagram in Fig. 1 is depicted with the mol fraction x, but the concentration profile in Fig. 2 is drawn with the

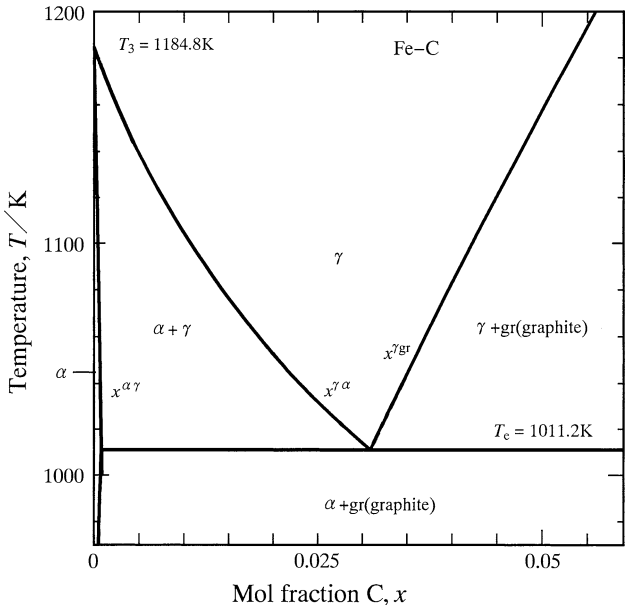

Fig. 1 The equilibrium phase diagram in the binary Fe–C system thermodynamically evaluated by Gustafson [67]

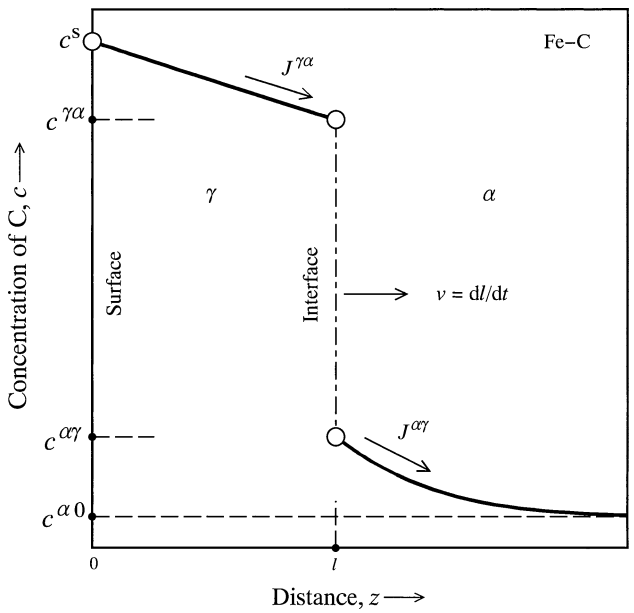

Fig. 2 The schematic concentration profile of C along the diffusional direction across the γ phase formed on the surface of the α phase

concentration c. However, x is readily converted into c by the relationship $c = x/V_m$, where V_m is the molar volume of the relevant phase. The value of c corresponding to $x^{\alpha 0}$ is denoted by $c^{\alpha 0}$ in Fig. 2. In this figure, c^s is the composition on the surface of the γ phase, and $c^{\gamma\alpha}$ and $c^{\alpha\gamma}$ are those in the γ and α phases, respectively, at the γ/α interface. For the diffusion controlling migration, the local equilibrium is realized at the γ/α interface and the surface. Under such conditions, $c^{\gamma\alpha}$ and $c^{\alpha\gamma}$ coincide with the corresponding compositions of the two-phase γ/α tie-line, and c^s, $c^{\gamma\alpha}$, and $c^{\alpha\gamma}$ remain constant during isothermal annealing. Hence, the migration rate $v = dl/dt$ of the γ/α interface is related with the flux balance at the interface as follows [52].

$$(c^{\gamma\alpha} - c^{\alpha\gamma})v = J^{\gamma\alpha} - J^{\alpha\gamma} \tag{1}$$

Here, $J^{\alpha\gamma}$ and $J^{\gamma\alpha}$ are the diffusional fluxes of C due to the volume diffusion in the α and γ phases, respectively, at the interface. According to Fick's first law, the diffusional flux J^ϕ is proportional to the concentration gradient $\partial c^\phi/\partial z$ as follows.

$$J^\phi = -D^\phi\left(\frac{\partial c^\phi}{\partial z}\right)(\phi = \alpha, \gamma) \tag{2}$$

In Eq. 2, D^ϕ is the diffusion coefficient for volume diffusion of C in the ϕ phase, and ϕ stands for α and γ. If the diffusion coefficient D^ϕ varies depending on the composition c^ϕ of the ϕ phase, Fick's second law is described by the following equation.

$$\frac{\partial c^\phi}{\partial t} = \frac{\partial}{\partial z}\left(D^\phi\frac{\partial c^\phi}{\partial z}\right) = D^\phi\frac{\partial^2 c^\phi}{\partial z^2} + \frac{\partial D^\phi}{\partial c^\phi}\left(\frac{\partial c^\phi}{\partial z}\right)^2(\phi = \alpha, \gamma) \tag{3}$$

Equation 3 indicates that the composition c^ϕ is a function of the distance z and the annealing time t. The initial condition is expressed by the equation

$$c^\alpha(z > 0, t = 0) = c^{\alpha 0}, \tag{4}$$

and the boundary conditions are described as

$$c^\gamma(z = 0, t > 0) = c^s, \tag{5a}$$

$$c^\gamma(z = l, t > 0) = c^{\gamma\alpha}, \tag{5b}$$

$$c^\alpha(z = l, t > 0) = c^{\alpha\gamma} \tag{5c}$$

and

$$c^\alpha(z = \infty, t > 0) = c^{\alpha 0}. \tag{5d}$$

Unfortunately, however, no analytical solution is known for Eqs. 1–3 under the initial and boundary conditions of Eqs. 4 and 5. Therefore, Eqs. 1–3 will be solved numerically. For the numerical calculation, Crank–Nicolson implicit method [68] was combined with a finite-difference technique [69] in a manner similar to previous studies [64, 65]. In the finite-difference technique, the distance z and the annealing time t are divided into intervals Δz and Δt, respectively, and then described as $z_i = i\Delta z$ and $t_j = j\Delta t$, respectively. Here, i and j are the dimensionless integers that are equal to or greater than 0. The concentration profile of C along the diffusional direction in the γ and α phases at $t = t_j$ is schematically shown in Fig. 3. In this figure, the ordinate and the abscissa indicate c and z, respectively, and l is the thickness of the γ phase and hence the position of the γ/α interface. In Fig. 3, l is divided into grid points with a number of $n + 1$. The interval Δz^γ between the neighboring grid points in the γ phase is obtained by the relationship $\Delta z^\gamma = l/n$. Thus, $z_i^\gamma = i\Delta z^\gamma$ for $0 \le i \le n$. The composition of the γ phase at $z = z_i^\gamma$ and $t = t_j$ is denoted by $c_{i,j}^\gamma$. On the other hand, the interval Δz^α for the α phase is calculated by the relationship $\Delta z^\alpha = (L - l)/m$. Here, L is the fixed position where c^α is equal to $c^{\alpha 0}$ even at the longest annealing time. Hence, L should be much greater than l. Also for the α phase, the composition at $z = z_i^\alpha$ and $t = t_j$ is denoted by $c_{i,j}^\alpha$. As shown in Fig. 3, however, the incremental direction of i for $c_{i,j}^\alpha$ is opposite to that for $c_{i,j}^\gamma$. Therefore, $c_{0,j}^\gamma = c_{0,0}^\gamma = c^s$ at $z = 0$, $c_{n,j}^\gamma = c_{n,0}^\gamma = c^{\gamma\alpha}$ and $c_{m,j}^\alpha = c_{m,0}^\alpha = c^{\alpha\gamma}$ at $z = l$, $c_{0,j}^\alpha = c_{0,0}^\alpha = c^{\alpha 0}$ at $z = L$, and $z_i^\alpha = L - i\Delta z^\alpha$ for $0 \le i \le m$. Consequently, we obtain

$$\begin{aligned}4(1 + r^\phi)c_{1,j+1}^\phi - \left(p_i^\phi v_{j+1}^\phi + 2r^\phi\right)c_{2,j+1}^\phi \\ = \left(4r^\phi - p_i^\phi v_j^\phi - p_i^\phi v_{j+1}^\phi\right)c_{0,0}^\phi + 4(1 - r^\phi)c_{1,j}^\phi \\ + \left(p_i^\phi v_j^\phi + 2r^\phi\right)c_{2,j}^\phi + r_c^\phi\left(c_{2,j}^\phi - c_{0,j}^\phi\right)^2\end{aligned} \tag{6a}$$

for $i = 1$,

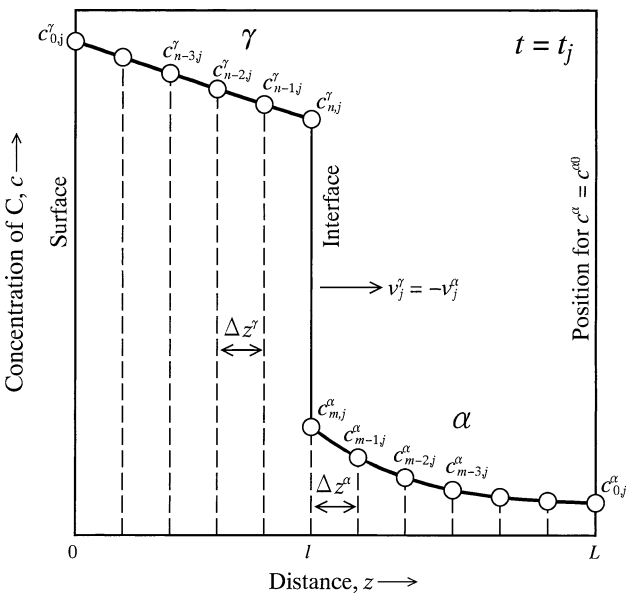

Fig. 3 The schematic concentration profile of C along the diffusional direction in the γ and α phases at $t = t_j$

$$\left(p_i^{\phi}v_{j+1}^{\phi}-2r^{\phi}\right)c_{i-1,j+1}^{\phi}+4\left(1+r^{\phi}\right)c_{i,j+1}^{\phi} - \left(p_i^{\phi}v_{j+1}^{\phi}+2r^{\phi}\right)c_{i+1,j+1}^{\phi}=\left(2r^{\phi}-p_i^{\phi}v_j^{\phi}\right)c_{i-1,j}^{\phi} +4\left(1-r^{\phi}\right)c_{i,j}^{\phi}+\left(p_i^{\phi}v_j^{\phi}+2r^{\phi}\right)c_{i+1,j}^{\phi}+r_c^{\phi}\left(c_{i+1,j}^{\phi}-c_{i-1,j}^{\phi}\right)^2 \tag{6b}$$

for $1 < i < k-1$, and

$$\left(p_i^{\phi}v_{j+1}^{\phi}-2r^{\phi}\right)c_{k-2,j+1}^{\phi}+4\left(1+r^{\phi}\right)c_{k-1,j+1}^{\phi} =\left(2r^{\phi}-p_i^{\phi}v_j^{\phi}\right)c_{k-2,j}^{\phi}+4\left(1-r^{\phi}\right)c_{k-1,j}^{\phi} +\left(p_i^{\phi}v_j^{\phi}+p_i^{\phi}v_{j+1}^{\phi}+4r^{\phi}\right)c_{k,0}^{\phi}+r_c^{\phi}\left(c_{k,j}^{\phi}-c_{k-2,j}^{\phi}\right)^2 \tag{6c}$$

for $i = k-1$. Here, r^{ϕ}, r_c^{ϕ} and p_i^{ϕ} are defined as

$$r^{\phi}\equiv\frac{D^{\phi}\Delta t}{\left(\Delta z^{\phi}\right)^2}, \tag{7a}$$

$$r_c^{\phi}\equiv\frac{\partial D^{\phi}}{\partial c^{\phi}}\frac{\Delta t}{\left(\Delta z^{\phi}\right)^2} \tag{7b}$$

and

$$p_i^{\phi}\equiv\frac{i\Delta t}{k\Delta z^{\phi}}, \tag{7c}$$

respectively. In Eqs. 6 and 7, $k = m$ and n for $\phi = \alpha$ and γ, respectively. The migration rate v_j^{α} or v_j^{γ} of the γ/α interface at $t = t_j$ is obtained by the equation

$$v_j^{\gamma}=-v_j^{\alpha} =q^{\alpha}\left(3c_{m,0}^{\alpha}-4c_{m-1,j}^{\alpha}+2c_{m-2,j}^{\alpha}\right) +q^{\gamma}\left(3c_{n,0}^{\gamma}-4c_{n-1,j}^{\gamma}+2c_{n-2,j}^{\gamma}\right), \tag{8}$$

where q^{α} and q^{γ} are defined as

$$q^{\alpha}\equiv\frac{D^{\alpha}}{2\left(c_{m,0}^{\alpha}-c_{n,0}^{\gamma}\right)\Delta z^{\alpha}} \tag{9a}$$

and

$$q^{\gamma}\equiv\frac{D^{\gamma}}{2\left(c_{m,0}^{\alpha}-c_{n,0}^{\gamma}\right)\Delta z^{\gamma}}, \tag{9b}$$

respectively. Equation 6 is simply described with matrices $\boldsymbol{A}$, $\boldsymbol{B}$, and $\boldsymbol{C}$ as follows.

$$\boldsymbol{AC}=\boldsymbol{B} \tag{10}$$

Here,

$$\boldsymbol{A}=\begin{pmatrix} 4\left(1+r^{\phi}\right) & -p_1v_{j+1}^{\phi}-2r^{\phi} & 0 & \cdots & 0 & 0\\ p_2v_{j+1}^{\phi}-2r^{\phi} & 4\left(1+r^{\phi}\right) & -p_2v_{j+1}^{\phi}-2r^{\phi} & \cdots & 0 & 0\\ 0 & p_3v_{j+1}^{\phi}-2r^{\phi} & 4\left(1+r^{\phi}\right) & \cdots & 0 & 0\\ \vdots & \vdots & \vdots & \ddots & \vdots & \vdots\\ 0 & 0 & 0 & p_{k-2}v_{j+1}^{\phi}-2r^{\phi} & 4\left(1+r^{\phi}\right) & -p_{k-2}v_{j+1}^{\phi}-2r^{\phi}\\ 0 & 0 & 0 & 0 & p_{k-1}v_{j+1}^{\phi}-2r^{\phi} & 4\left(1+r^{\phi}\right) \end{pmatrix}, \tag{11a}$$

$$\boldsymbol{B}=\begin{pmatrix} \left(4r^{\phi}-p_1^{\phi}v_j^{\phi}-p_1^{\phi}v_{j+1}^{\phi}\right)c_{0,0}^{\phi}+4\left(1-r^{\phi}\right)c_{1,j}^{\phi}+\left(2r^{\phi}+p_1^{\phi}v_j^{\phi}\right)c_{2,j}^{\phi}+r_c^{\phi}\left(c_{0,j}^{\phi}-c_{2,j}^{\phi}\right)^2\\ \left(2r^{\phi}-p_2^{\phi}v_j^{\phi}\right)c_{1,j}^{\phi}+4\left(1-r^{\phi}\right)c_{2,j}^{\phi}+\left(2r^{\phi}+p_2^{\phi}v_j^{\phi}\right)c_{3,j}^{\phi}+r_c^{\phi}\left(c_{1,j}^{\phi}-c_{3,j}^{\phi}\right)^2\\ \left(2r^{\phi}-p_3^{\phi}v_j^{\phi}\right)c_{2,j}^{\phi}+4\left(1-r^{\phi}\right)c_{3,j}^{\phi}+\left(2r^{\phi}+p_3^{\phi}v_j^{\phi}\right)c_{4,j}^{\phi}+r_c^{\phi}\left(c_{2,j}^{\phi}-c_{4,j}^{\phi}\right)^2\\ \vdots\\ \left(2r^{\phi}-p_{k-2}^{\phi}v_j^{\phi}\right)c_{k-3,j}^{\phi}+4\left(1-r^{\phi}\right)c_{k-2,j}^{\phi}+\left(2r^{\phi}+p_{k-2}^{\phi}v_j^{\phi}\right)c_{k-1,j}^{\phi}+r_c^{\phi}\left(c_{k-3,j}^{\phi}-c_{k-1,j}^{\phi}\right)^2\\ \left(2r^{\phi}-p_{k-1}^{\phi}v_j^{\phi}\right)c_{k-2,j}^{\phi}+4\left(1-r^{\phi}\right)c_{k-1,j}^{\phi}+\left(4r^{\phi}+p_{k-1}^{\phi}v_j^{\phi}+p_{k-1}^{\phi}v_{j+1}^{\phi}\right)c_{k,0}^{\phi}+r_c^{\phi}\left(c_{k-2,j}^{\phi}-c_{k,j}^{\phi}\right)^2 \end{pmatrix} \tag{11b}$$

and

$$\boldsymbol{C} = \begin{pmatrix} c^{\phi}_{1,j+1} \\ c^{\phi}_{2,j+1} \\ c^{\phi}_{3,j+1} \\ \vdots \\ c^{\phi}_{k-2,j+1} \\ c^{\phi}_{k-1,j+1} \end{pmatrix}. \tag{11c}$$

The matrix $\boldsymbol{C}$ consisting of the unknown composition $c^{\phi}_{i,j+1}$ is calculated for the matrix $\boldsymbol{B}$ containing the known composition $c^{\phi}_{i,j}$ from Eq. 10. As can be seen in Eq. 11a, the matrix $\boldsymbol{A}$ is tridiagonal. Hence, the calculation can be easily conducted by an appropriate linear algebra technique even for a large number of k [70].

Results and discussion

Diffusion coefficient

The diffusion coefficient D^{γ} of C in the γ phase of the binary Fe–C system was experimentally determined by Wells et al. [62] and Smith [63]. Their experimental results indicate that D^{γ} varies depending on the composition of the γ phase as well as the temperature. On the basis of their results, the dependence of D^{γ} on the composition and the temperature was quantitatively analyzed by various researchers [71–73]. According to a recent analysis by Ågren [73], D^{γ} is mathematically expressed as a function of y and T by the following equation.

$$D^{\gamma}(y) = 4.53 \times 10^{-7}\left\{1 + \frac{8339.9y(1-y)}{T}\right\} \times \exp\left\{-\left(\frac{1}{T} - 2.221 \times 10^{-4}\right)(17767 - 26436y)\right\}. \tag{12}$$

Here, y is the site fraction of C in the interstitial site of the γ phase, and D^{γ} is measured in m^2/s. The term $D^{\gamma}(y)$ explicitly indicates that D^{γ} is a function of y. The site fraction y is related with the mol fraction x by the equation

$$y = \frac{x}{1-x}. \tag{13}$$

If D^{γ} is evaluated using x instead of y, D^{γ} is denoted by $D^{\gamma}(x)$. For practical purposes, $D^{\gamma}(x)$ is approximately related with $D^{\gamma}(y)$ by the following equation [72].

$$D^{\gamma}(x) = (1+y)D^{\gamma}(y) \tag{14}$$

The dependence of D^{γ} on x and T in the γ single-phase region was calculated from Eqs. 12–14. The result is shown as solid curves in Fig. 4. In this figure, the abscissa indicates x, and the ordinate shows the logarithm of D^{γ}. As can be seen, D^{γ} monotonically increases with increasing values of x and T.

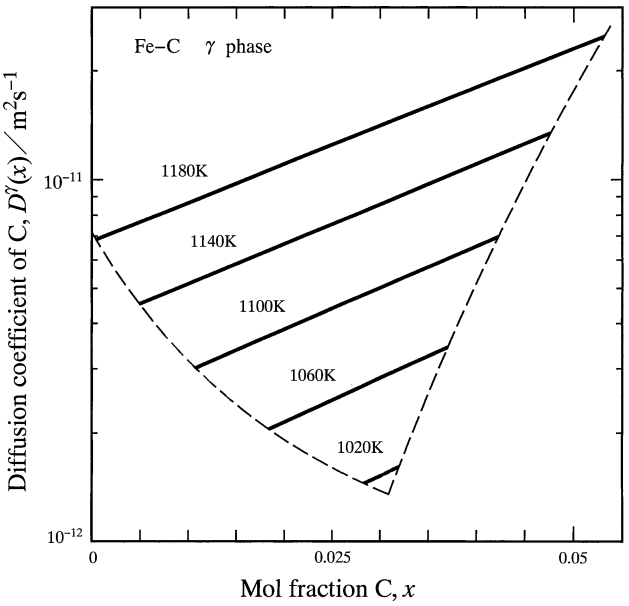

Fig. 4 The diffusion coefficient $D^{\gamma}(x)$ of C in the γ phase versus the mol fraction x of C at $T = 1020$–1180 K calculated from Eqs. 12–14

In contrast, as shown in Fig. 1, the solubility of C in the α phase is very small. Consequently, unlike D^{γ}, D^{α} is considered independent of the composition. In such a case, D^{α} is expressed as a function of T by an ordinary Arrhenius equation as follows.

$$D^{\alpha} = D^{\alpha}_0 \exp\left(-\frac{Q^{\alpha}}{RT}\right) \tag{15}$$

Here, D^{α}_0 is the pre-exponential factor, Q^{α} is the activation enthalpy, and R is the gas constant. According to a literature [74], D^{α}_0 is constant as

$$D^{\alpha}_0 = 1.24 \times 10^{-5}\ \mathrm{m^2/s}, \tag{16a}$$

but Q^{α} slightly varies depending on T as

$$Q^{\alpha} = 99.5\left(1 - \frac{30.9}{T}\right)\mathrm{kJ/mol}. \tag{16b}$$

Migration behavior of γ/α interface

According to the equilibrium phase diagram in the binary Fe–C system of Fig. 1 [67], the temperature dependence of the mol fraction $x^{\phi\theta}$ of C for the $\phi/(\phi + \theta)$ phase boundary is expressed by the following equation in the temperature range between $T = T_e = 1011.2$ K and $T = T_3 = 1184.8$ K.

$$x^{\phi\theta} = a_0 + a_1 T + a_2 T^2 + a_3 T^3 \tag{17}$$

The values of the coefficient a_h ($h = 0, 1, 2, 3$) for $x^{\alpha\gamma}$, $x^{\gamma\alpha}$, and $x^{\gamma gr}$ are listed at the second, third, and fourth columns, respectively, in Table 1. From Eqs. 12–16, $D^{\gamma} = 7.20 \times 10^{-12}$ m^2/s and $D^{\alpha} = 6.63 \times 10^{-10}$ m^2/s are calculated at $T = T_3$ and $x = 0$. On the other hand, the

Table 1 Values of the coefficient a_h ($h = 0, 1, 2, 3$) in Eq. 17 for $x^{\alpha\gamma}$, $x^{\gamma\alpha}$, and $x^{\gamma gr}$ in Fig. 1

	$x^{\alpha\gamma}$	$x^{\gamma\alpha}$	$x^{\gamma gr}$
a_0	3.458780×10^{-2}	2.605633	4.747339×10^{-2}
a_1	-8.803226×10^{-5}	-6.119819×10^{-3}	-2.305500×10^{-4}
a_2	7.957676×10^{-8}	4.844269×10^{-6}	2.856705×10^{-7}
a_3	$-2.524968 \times 10^{-11}$	-1.295752×10^{-9}	$-7.307500 \times 10^{-11}$

molar volumes of the α and γ phases are estimated to be $V_m^\alpha = 7.37 \times 10^{-6}$ m^3/mol and $V_m^\gamma = 7.30 \times 10^{-6}$ m^3/mol from the lattice parameters $a^\alpha = 0.2904$ nm and $a^\gamma = 0.3647$ nm of the α and γ phases, respectively, at $T = T_3$ and $x = 0$ [75]. Hence, we obtain the ratios of $D^\alpha/D^\gamma = 92$ and $V_m^\alpha/V_m^\gamma = 1.01$. Although these ratios will slightly vary depending on the temperature and the compositions of the α and γ phases, the difference between V_m^α and V_m^γ is negligible compared with that between D^α and D^γ. Consequently, we may assume that V_m^α and V_m^γ are equal to each other and independent of the temperature and the composition. Owing to this assumption, the concentration c is automatically replaced with the mol fraction x in Eqs. 4–11. From these equations, the migration of the γ/α interface was numerically calculated at the temperatures of $T = 1020$–1180 K.

If the second term on the right-hand side of Eq. 3 is negligible, Eqs. 1–3 can be analytically solved under the initial and boundary conditions of Eqs. 4 and 5 [52]. In such a hypothetical case, $x_{i,j}^\phi$ at $t_j = 1$ s was evaluated by the analytical solution using a value of D^γ obtained at $x = x^{\gamma\alpha}$. The evaluation was utilized as the starting value of the numerical calculation at $t_j = 1$ s. The numerical calculation was iterated up to $t_{j+1} = 4 \times 10^4$ s. During the iteration, the position of the γ/α interface $z = l$ varies depending on the annealing time t, but the positions $z = 0$ and $z = L$ are fixed. As a result, Δz^α and Δz^γ change depending on t. However, an appropriate constant value of Δt was chosen to satisfy $r^\alpha < 0.5$ and $r^\gamma < 0.5$ in Eq. 7a. Furthermore, a sufficiently large value of L was selected to realize the following relationship for $t_{j+1} = 4 \times 10^4$ s at each temperature.

$$\left| x_{0,j+1}^\alpha - x_{0,0}^\alpha \right| < 10^{-10} \tag{18}$$

The result with $x^{\alpha 0} = 0$ and $x^s = x^{\gamma gr}$ is shown in Fig. 5. Here, x^s and $x_{i,j}^\phi$ are the mol fractions of C corresponding to the concentrations c^s and $c_{i,j}^\phi$, respectively. In this figure, the ordinate and the abscissa indicate the logarithms of l and t, respectively, and the values of l at representative annealing times are plotted as open circles. As can be seen, the plotted points are located well on parallel straight lines. Each straight line indicates the parabolic relationship between l and t described as follows.

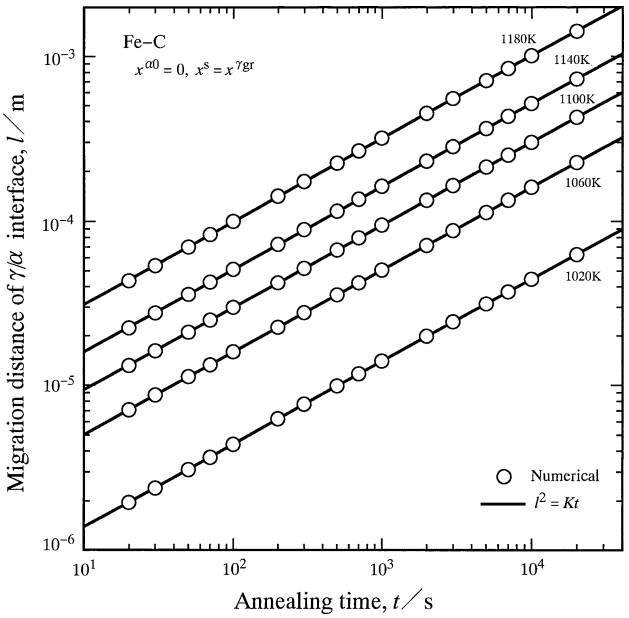

Fig. 5 The migration distance l of the γ/α interface versus the annealing time t at $T = 1020$–1180 K by the numerical calculation shown as *open circles*. *Parallel solid lines* indicate the parabolic relationship of Eq. 19

$$l^2 = Kt \tag{19}$$

The parabolic coefficient K in Eq. 19 is plotted as open circles against the temperature T in Fig. 6. In this figure, the ordinate indicates the logarithm of K, and the abscissa shows the reciprocal of T. The temperature dependence of

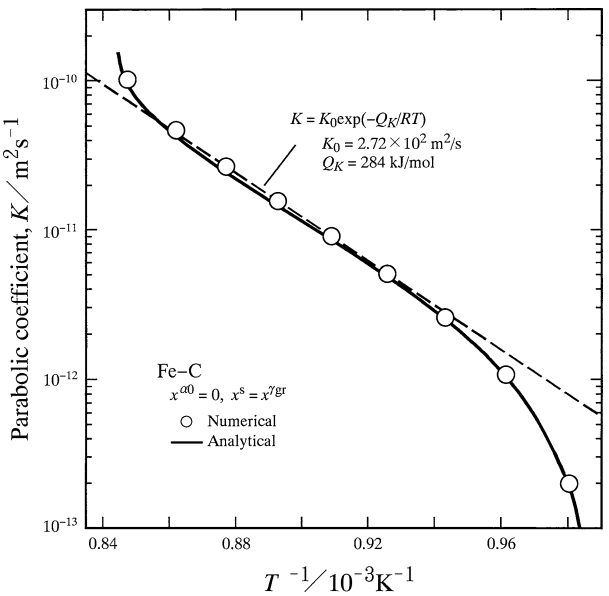

Fig. 6 The parabolic coefficient K versus the temperature T by the numerical calculation shown as *open circles*. A *solid curve* indicates the corresponding result obtained from the analytical solution reported by Jost [52]

K may be expressed by an Arrhenius equation with certain accuracy as follows [54–56].

$$K = K_0 \exp\left(-\frac{Q_K}{RT}\right) \tag{20}$$

Here, K_0 and Q_K are the pre-exponential factor and the activation enthalpy, respectively. As can be seen in Fig. 6, K monotonically increases with increasing temperature T. In the temperature range of $T = 1080$–1140 K, the open circles lie well on a straight-dashed line. Thus, in this temperature range, the temperature dependence of K is described by Eq. 20. The dashed line gives $K_0 = 2.72 \times 10^2$ m^2/s and $Q_K = 284$ kJ/mol. On the other hand, the open circles are located on the upper side of the dashed line at $T > 1140$ K, but on the lower side of the dashed line at $T < 1080$ K. Such a complicated temperature dependency of K was recognized also for the growth of the γ phase due to the reactive diffusion between the Fe-rich α_1 phase and the Cr-rich α_2 phase in the binary Fe–Cr system [59]. As shown in Fig. 1, the solubility range of the γ phase in the binary Fe–C system varies depending on the temperature. In such a case, Q_K cannot be necessarily correlated with the activation enthalpy of the diffusion coefficient in a straightforward manner even at $T = 1080$–1140 K [60]. On the other hand, a solid curve in Fig. 6 shows the corresponding result obtained by the analytical solution mentioned above. As can be seen, the open circles are close to the solid curve, but located slightly on the upper side of the solid curve. For a comparison of K between the open circle and the solid curve, the ratio r_K of K_n to K_a is defined as

$$r_K = \frac{K_n}{K_a}. \tag{21}$$

Here, K_n is the value of the numerical calculation, and K_a is that of the analytical solution. The values of r_K calculated from Eq. 21 are plotted as open circles against the temperature T in Fig. 7. As can be seen, r_K is nearly equal to unity at temperatures slightly higher than $T = T_e = 1011.2$ K, but gradually increases with increasing temperature. After reaching to the maximum value at $T \cong 1160$ K, r_K slightly decreases with increasing temperature up to $T = T_3 = 1184.8$ K. Therefore, the composition dependence of the diffusion coefficient of C in the γ phase results in acceleration of the migration of the γ/α interface at higher temperatures. Nevertheless, the maximum value of r_K is merely 1.11. Hence, the influence is at most 11% of acceleration.

Comparison with observation

As mentioned in "Introduction" section, the carburization of Fe was experimentally observed by Togashi and Nishizawa [61]. In this experiment, the α phase of pure Fe was isothermally annealed at 1073 K for various times up to 9 h in a carburization atmosphere with the same activity of C as graphite. Owing to annealing, the γ phase is produced on the α phase, and gradually grows into the α phase. The experimental values for the migration distance l of the γ/α interface are plotted as open symbols against the annealing time t in Fig. 8. In this figure, the ordinate and

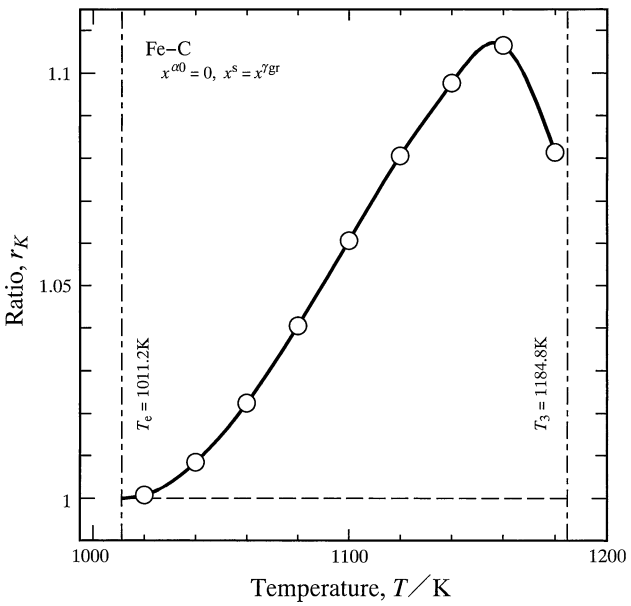

Fig. 7 The ratio r_K versus the temperature T for the numerical and analytical calculations in Fig. 6

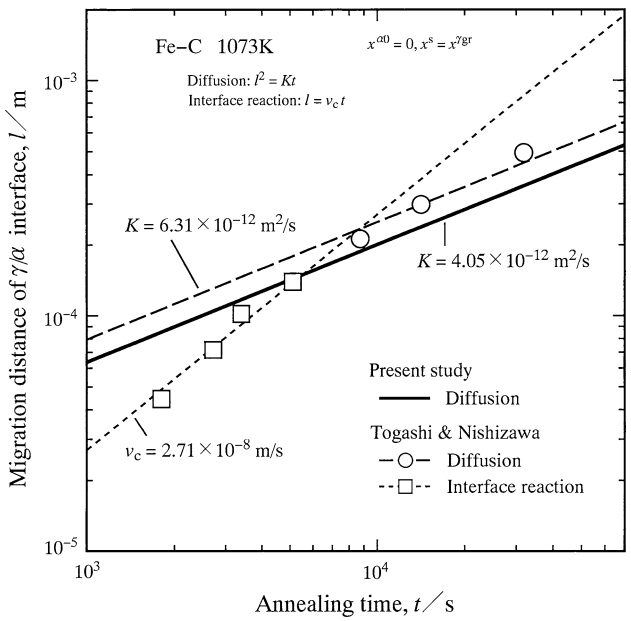

Fig. 8 The migration distance l of the γ/α interface versus the annealing time t at $T = 1073$ K by the numerical calculation shown as a *solid line*. *Open symbols* indicate the experimental result by Togashi and Nishizawa [61], and *dashed and dotted lines* show the calculations by Eqs. 19 and 22, respectively

the abscissa indicate the logarithms of l and t, respectively, and open squares and circles show the values of l at shorter and longer annealing times, respectively. Although the plotted points are slightly scattered, l is proportional to t for the open squares, but l^2 is proportional to t for the open circles. Hence, the parabolic relationship holds in the late stages of the migration. For the open circles, $K = 6.31 \times 10^{-12}$ m^2/s is evaluated from Eq. 19 by the least-squares method. In contrast, the proportional relationship in the early stages of the migration is described as follows.

$$l = v_c t \tag{22}$$

Here, v_c is the proportionality coefficient that corresponds to the migration rate of the γ/α interface independent of the annealing time t. For the open squares, $v_c = 2.71 \times 10^{-8}$ m/s is estimated from Eq. 22 by the least-squares method. The dependencies of l on t calculated from Eqs. 19 and 22 using $K = 6.31 \times 10^{-12}$ m^2/s and $v_c = 2.71 \times 10^{-8}$ m/s are shown as dashed and dotted lines, respectively, in Fig. 8. The dashed and dotted lines intersect at $t = 8.6$ ks. Therefore, it is concluded that the migration of the γ/α interface during the isothermal carburization at $T = 1073$ K is controlled by the interface reaction in the migrating interface at $t < 8.6$ ks but by the volume diffusion of C in the α and γ phases at $t > 8.6$ ks. The transition of the rate controlling process from the interface reaction to the volume diffusion was experimentally observed also for the growth of a Ta–Sn compound due to the reactive diffusion between Ta and a bronze in a previous study [76]. On the other hand, the result of the numerical calculation at $T = 1073$ K is shown as a solid line in Fig. 8. As can be seen, agreement between the solid line and the dashed line is satisfactory.

For the migration controlled by the interface reaction, the migration rate v_c is related with the driving force ΔG_m as follows.

$$v_c = M \Delta G_m \tag{23}$$

Here, M is the mobility of the interface. The temperature dependence of M is described by the following equation of the same formula as Eqs. 15 and 20.

$$M = M_0 \exp\left(-\frac{Q_M}{RT}\right) \tag{24}$$

The pre-exponential factor and the activation enthalpy for the migration of the γ/α interface in Fe are reported to be $M_0 = 5.8 \times 10^{-5}$ mol m/J s and $Q_M = 140$ kJ/mol by Krielaart et al. [77] These parameters provide $M = 8.88 \times 10^{-12}$ molm/J s at $T = 1073$ K. Inserting $M = 8.88 \times 10^{-12}$ molm/Js and $v_c = 2.71 \times 10^{-8}$ m/s into Eq. 23, we obtain $\Delta G_m = 3.05$ kJ/mol. This value is the driving force for the migration of the γ/α interface controlled by the interface reaction under the given experimental conditions. The transition of the rate controlling process from the interface reaction to the volume diffusion was numerically analyzed for the migration of the γ/α interface owing to the isothermal precipitation of the α phase in the γ phase of the binary Fe–C system by Krielaart et al. [77]. During the precipitation, the volume fraction of the α phase gradually increases with increasing annealing time, but the total amount of C in the specimen remains constant independent of the annealing time. Under such conditions, the nonequilibrium compositions of the α and γ phases at the migrating interface for the interface reaction were numerically estimated as functions of the annealing time. On the other hand, in the case of the carburization, the total amount of C in the specimen monotonically increases with increasing annealing time. Consequently, their numerical model cannot be readily applied to the carburization.

The concentration profile of C in the γ phase at $T = 1073$ K for $t = 4$ h reported by Togashi and Nishizawa [61] is shown as open circles in Fig. 9. On the other hand, solid curves indicate the corresponding result of the numerical calculation in the present study. Furthermore, open squares show $x^{\alpha\gamma}$ and $x^{\gamma\alpha}$, and a vertical dashed and dotted line represents the position of the γ/α interface. As shown in Fig. 8, the migration rate of the γ/α interface is slightly smaller for the numerical calculation than for the observation. Hence, the γ/α interface for the open circles should be located lightly on the right-hand side of the dashed and dotted line. For direct comparison of the concentration profile, however, the position of the interface for

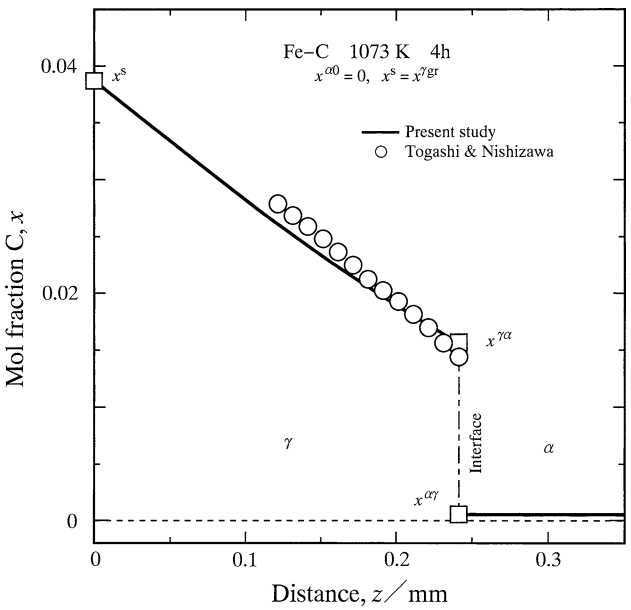

Fig. 9 The concentration profile of C along the diffusional direction across the γ phase at $T = 1073$ K for $t = 4$ h by the numerical calculation shown as *solid curves*, *open squares*, and a *dashed and dotted line*. *Open circles* indicate the experimental result by Togashi and Nishizawa [61]

the observation is adjusted to that for the numerical calculation in Fig. 9. As can be seen, agreement of the concentration profile between the numerical calculation and the observation is also satisfactory. Consequently, the numerical calculation quantitatively reproduces the diffusion controlling migration of the γ/α interface during the isothermal carburization in the binary Fe–C system.

Conclusions

The migration behavior of the γ/α interface due to isothermal carburization of the bcc-α phase in the binary Fe–C system at the temperatures of $T = 1020$–1180 K was numerically analyzed using the diffusion equation describing the flux balance at the migrating interface. During the isothermal carburization, the fcc-γ phase is formed as a uniform layer on a flat surface of the α phase, and then grows toward the α phase. For the γ phase, the diffusion coefficient D^{γ} of C monotonically increases with increasing concentration of C [62, 63]. Hence, in the numerical analysis, D^{γ} was expressed as a function of the composition as well as the temperature. The numerical analysis indicates that the square of the migration distance l of the γ/α interface is proportional to the annealing time t as $l^2 = Kt$. The parabolic coefficient K increases with increasing temperature T but varies in a complicated manner. Thus, the temperature dependence of K cannot be simply expressed by an ordinary Arrhenius equation. The composition dependence of D^{γ} causes acceleration of the migration of the γ/α interface. However, the influence of acceleration is at most 11%. The numerical analysis quantitatively reproduces the diffusion controlling migration of the γ/α interface during the isothermal carburization of pure Fe at $T = 1073$ K observed by Togashi and Nishizawa [61].

Acknowledgement This study was supported by the Iketani Science and Technology Foundation in Japan.

References

1. Lustman B, Mehl RF (1942) Trans Met Soc AIME 147:369
2. Horstmann D (1953) Stahl Eisen 73:659
3. Storchheim S, Zambrow JL, Hausner HH (1954) Trans Met Soc AIME 200:269
4. Peterson NL, Ogilvie RE (1960) Trans Met Soc AIME 218:439
5. Kidson GV, Miller GD (1964) J Nucl Mater 12:61
6. Shibata K, Morozumi S, Koda S (1966) J Jpn Inst Met 30:382
7. Hirano K, Ipposhi Y (1968) J Jpn Inst Met 32:815
8. Funamizu Y, Watanabe K (1971) Trans JIM 12:147
9. Janssen MMP (1973) Metall Trans 4:1623
10. Bastin GF, Rieck GD (1974) Metall Trans 5:1817
11. Onishi M, Fujibuchi H (1975) Trans JIM 16:539
12. Iijima Y, Igarashi T, Hirano K (1979) J Mater Sci 14:474. doi:10.1007/BF00589842
13. Williams DS, Rapp RA, Hirth JP (1981) Metall Trans A 12A:639
14. Osamura K, Ochiai S, Kondo S, Namatame M, Nosaki M (1986) J Mater Sci 21:1509. doi:10.1007/BF01114703
15. Hannech EI-B, Hall CR (1992) Mater Sci Technol 8:817
16. Bhanumurthy K, Kale GB (1993) J Mater Sci Lett 12:1879
17. Lorenz M, Bergner D, Baum H (1994) Fresenius J Anal Chem 349:253
18. Vianco PT, Hlava PF, Kilgo AL (1994) J Electron Mater 23:583
19. Dybkov VI, Duchenko OV (1996) J Alloys Compd 234:295
20. Watanabe M, Horita Z, Nemoto M (1997) Interface Sci 4:229
21. Tortorici PC, Dayananda MA (1999) Metall Mater Trans A 30A:545
22. Choi S, Bieler TR, Lucas JP, Subramanian KN (1999) J Electron Mater 28:1209
23. Duchenko OV, Vereshchaka VM, Dybkov (1999) J Alloys Compd 288:164
24. van Dal MJH, Huibers DGGM, Kodentsov AA, van Loo FJJ (2001) Intermetallics 9:409
25. Milanese C, Buscaglia V, Maglia F, Anselmi-Tamburini U (2002) Acta Mater 50:1393
26. Taguchi O, Tiwari GP, Iijima Y (2003) Mater Trans 44:83
27. Kajihara M, Yamada T, Miura K, Kurokawa N, Sakamoto K (2003) Netsushori 43:297
28. Paul A, Kodentsov AA, de With G, van Loo FJJ (2003) Intermetallics 11:1195
29. Yamada T, Miura K, Kajihara M, Kurokawa N, Sakamoto K (2004) J Mater Sci 39:2327. doi:10.1023/B:JMSC.0000019993.32079.c2
30. Tryon B, Feng Q, Pollock T (2004) Intermetallics 12:957
31. Yamada T, Miura K, Kajihara M, Kurokawa N, Sakamoto K (2005) Mater Sci Eng A 390:118
32. Takenaka T, Kano S, Kajihara M, Kurokawa N, Sakamoto K (2005) Mater Sci Eng A 396:115
33. Suzuki K, Kano S, Kajihara M, Kurokawa N, Sakamoto K (2005) Mater Trans 46:969
34. Takenaka T, Kano S, Kajihara M, Kurokawa N, Sakamoto K (2005) Mater Trans 46:1825
35. Mita M, Kajihara M, Kurokawa N, Sakamoto K (2005) Mater Sci Eng A 403:269
36. Muranishi Y, Kajihara M (2005) Mater Sci Eng A 404:33
37. Takenaka T, Kajihara M, Kurokawa N, Sakamoto K (2005) Mater Sci Eng A 406:134
38. Hayashi T, Ito K, Numakura H (2005) Intermetallics 13:93
39. Mita M, Miura K, Takenaka T, Kajihara M, Kurokawa N, Sakamoto K (2006) Mater Sci Eng B 126:37
40. Takenaka T, Kajihara M (2006) Mater Trans 47:822
41. Yato Y, Kajihara M (2006) Mater Trans 47:2277
42. Takenaka T, Kajihara M, Kurokawa N, Sakamoto K (2006) Mater Sci Eng A 427:210
43. Yato Y, Kajihara M (2006) Mater Sci Eng A 428:276
44. Hayase T, Kajihara M (2006) Mater Sci Eng A 433:83
45. Tanaka Y, Kajihata M, Watanabe Y (2006) Mater Sci Eng A 445–446:355
46. Furuto A, Kajihara M (2006) Mater Sci Eng A 445–446:604
47. Naoi D, Kajihara M (2007) Mater Sci Eng A 459:375
48. Sasaki S, Kajihara M (2007) Mater Trans 48:2642
49. Mikami K, Kajihara M (2007) J Mater Sci 42:8178. doi:10.1007/s10853-007-1700-0
50. Kajihara M, Takenaka T (2007) Mater Sci Forum 539–543:2473
51. Kajihara M, Sakama T (2007) Proceedings of the 13th symposium microjoining assembly tech electronics. Microjoining Commission, Yokohama, p 187
52. Jost W (1960) Diffusion of solids, liquids, gases. Academic Press, New York, p 68
53. Kajihara M (2004) Acta Mater 52:1193
54. Kajihara M (2005) Mater Sci Eng A 403:234

55. Kajihara M (2005) Mater Trans 46:2142
56. Kajihara M (2006) Defect Diffus Forum 249:91
57. Kajihara M (2006) Mater Trans 47:1480
58. Tanaka Y, Kajihara M (2006) Mater Trans 47:2480
59. Kajihara M, Yamashina T (2007) J Mater Sci 42:2432. doi: 10.1007/s10853-006-1212-3
60. Kajihara M (2008) Mater Trans 49:715
61. Togashi F, Nishazawa T (1976) J Jpn Inst Met 40:12
62. Wells C, Batz W, Mehl RF (1950) Trans AIME J Met 188:553
63. Smith RP (1953) Acta Metall 1:578
64. Tanaka T, Kajihara M (2007) Mater Sci Eng A 459:101
65. Furuto A, Kajihara M (2008) Mater Trans 49:294
66. Ågren J (1979) Metall Trans A 10A:1847
67. Gustafson P (1985) Scand J Metall 14:259
68. Crank J (1979) The mathematics of diffusion. Oxford University Press, London, p 144
69. Tanzilli RA, Heckel RW (1968) Trans Met Soc AIME 242:2313
70. Dahlquist G, Björck Å (1974) Numerical methods. Prentice-Hall, Englewood Cliffs, NJ, p 137
71. Guy AG (1952) Trans Am Soc Met 44:382
72. Ågren J (1982) Acta Metall 30:841
73. Ågren J (1986) Scr Metall 20:1507
74. Metals Data Book (1993) Japan Institute of Metals, Maruzen, Tokyo, p 21
75. Metals Hand Book (2000) Japan Institute of Metals, Maruzen, Tokyo, p 473
76. Tejima Y (2008) Master of Engineering Thesis, Tokyo Institute of Technology
77. Krielaart GP, Sietsma J, van der Zwaag S (1997) Mater Sci Eng A 237:216